Structural Characteristics of the Redox-sensing Coiled Coil in the Voltage-gated H⁺ Channel*

Yuichiro Fujiwara[‡1], Kohei Takeshita[‡§], Atsushi Nakagawa[§¶], and Yasushi Okamura[‡¶]

From the ‡Department of Physiology, Graduate School of Medicine, §Research Center for State-of-the-Art Functional Protein Analysis, Institute for Protein Research, and ¶Graduate School of Frontier Biosciences, Osaka University, Osaka 565-0871, Japan

Background: A pair of Cys residues is present in the coiled-coil assembly domain in the Hv channel dimer.
Results: An intersubunit disulfide bond forms in a redox-dependent manner and stabilizes the dimeric assembly.
Conclusion: The Hv channel has a redox sensor in the cytoplasmic region.
Significance: Hv channels expressed in phagocytes may sense the redox condition in production of reactive oxygen species for repelling bacteria.

Oxidation is an important biochemical defense mechanism, but it also elicits toxicity; therefore, oxidation must be under strict control. In phagocytotic events in neutrophils, the voltage-gated H⁺ (Hv) channel is a key regulator of the production of reactive oxygen species against invading bacteria. The cytoplasmic domain of the Hv channel forms a dimeric coiled coil underpinning a dimerized functional unit. Importantly, in the alignment of the coiled-coil core, a conserved cysteine residue forms a potential intersubunit disulfide bond. In this study, we solved the crystal structures of the coiled-coil domain in reduced, oxidized, and mutated (Cys → Ser) states. The crystal structures indicate that a pair of Cys residues forms an intersubunit disulfide bond dependent on the redox conditions. CD spectroscopy revealed that the disulfide bond increases the thermal stability of the coiled-coil protein. We also reveal that two thiol modifier molecules are able to bind to Cys in a redox-dependent manner without disruption of the dimeric coiled-coil assembly. Thus, the biochemical properties of the cytoplasmic coiled-coil domain in the Hv channel depend on the redox condition, which may play a role in redox sensing in the phagosome.

Redox (reduction-oxidation) reactions are important biochemical reactions in bodily functions. The reactive oxygen species (ROS)[2] produced play important roles in cell signaling and homeostasis (1), but they also elicit cellular toxicity that causes disease (2–4). Phagocytes such as macrophages and neutrophils utilize ROS for the digestion of invading bacteria (5, 6), where the voltage-gated H⁺ channel (called the Hv channel) optimizes the activity of NADPH oxidase that produces ROS (see Fig. 1A) (7).

VSOP (voltage-sensor domain-only protein)/Hv1 is a recently identified molecular correlate of the Hv channel (8, 9) expressed in phagocytes and spermatozoa. VSOP/Hv1 functions as a dimer (10–12), and the dimerization elicits a strong voltage-dependent H⁺ conductance that keenly responds to the NADPH oxidase activity (13–15). We recently identified the dimeric assembly domain of VSOP/Hv1 and solved its high-resolution crystal structure (13). The structure shows that the C terminus of VSOP/Hv1 forms a parallel dimeric coiled-coil architecture that underpins channel dimerization from the cytoplasmic side. It is noteworthy that a pair of Cys residues sits opposite in the core of the coiled coil, suggesting a potential disulfide bond of the Hv channel dimer that is expressed in the fluctuating environment of oxidation-reduction (see Fig. 1B). In addition, Cys-245 is conserved in homeothermal mammals and birds but not in other lower animals (see Fig. 1B). It is extremely rare for Cys residues to be situated in the coiled-coil hydrophobic core (16). The intersubunit disulfide bond in the core of the coiled coil has been investigated using the GCN4 coiled coil, a yeast leucine zipper peptide, containing a series of Cys mutations by biochemical analysis and computer modeling (17). It was reported that some intersubunit disulfide bonds stabilize the coiled coil, whereas others destabilize the coiled coil (17). This study provided some clues to the role of the disulfide bond in the coiled-coil protein, but it also suggested that the effect is difficult to predict because the coiled-coil stability is based on the geometric strain mediated by the disulfide bond and the local/general flexibility of the molecule (17). Thus, structure-function analysis of the Cys at position 245 in the cytoplasmic coiled-coil domain is required. In this study, we analyzed the biochemical properties of the Cys residues in the coiled-coil domain of mouse VSOP/Hv1 and determined the redox-sensing function of the channel.

EXPERIMENTAL PROCEDURES

Cloning and Construct Design—We used a mouse Hv channel clone (mVSOP/Hv1) (9) for all experiments in this study. A DNA fragment corresponding to the mVSOP/Hv1 coiled-coil domain (residues 220–269) was amplified by PCR and ligated into a pET28 (EMD Millipore)-derived vector, pET28HMT, kindly provided by Dr. Daniel L. Minor, Jr. (University of Cali-

[1] To whom correspondence should be addressed: Integrative Physiology, Dept. of Physiology, Graduate School of Medicine, Osaka University, Yamadaoka 2-2, Suita, Osaka 565-0871, Japan. Tel.: 81-6-6879-3311; Fax: 81-6-6879-3319; E-mail: fujiwara@phys2.med.osaka-u.ac.jp.

[2] The abbreviations used are: ROS, reactive oxygen species; mVSOP, mouse VSOP; MBP, maltose-binding protein; MalPEG, maleimide-conjugated PEG.

fornia, San Francisco). The vector contained, in sequence, a hexahistidine tag, maltose-binding protein (MBP), and a cleavage site for the tobacco etch virus protease.

Protein Expression and Purification—His-tagged MBP fusion proteins were expressed in *Escherichia coli* BL21(DE3)pLysS cells grown in 2× yeast/Tryptone medium at 37 °C and induced with 0.4 mM isopropyl β-D-thiogalactopyranoside for 4 h. The cells were harvested by centrifugation, and the cell pellets were lysed by sonication in lysis buffer (10 mM K_2HPO_4 (pH 7.3), 250 mM KCl, and 1 mM PMSF). The soluble fraction was applied to a 20-ml HisPrep FF nickel-charged column (GE Healthcare) and eluted with 500 mM imidazole on an ÄKTA purifier system (GE Healthcare). The fusion proteins were then applied to a 75-ml amylose column (New England Biolabs) and eluted with 10 mM maltose, after which the maltose was removed on a 53-ml HiPrep desalting column (GE Healthcare). The His$_6$ tag and MBP were then cleaved with tobacco etch virus protease. Coiled-coil proteins were further purified on a Superdex 75 gel filtration column (GE Healthcare) for crystallization (see Fig. 3). The protein concentration was determined using the BCA protein assay kit (Thermo Fisher Scientific).

Crystallography—Coiled-coil domain proteins were crystallized at 10 °C by hanging-drop vapor diffusion. The crystals were grown from mixtures of 1 μl of protein solution (5 mg/ml protein dissolved in 150 mM KCl and 5 mM HEPES (pH 7.3)) and 1 μl of reservoir solution containing 100 mM KCl, 50 mM Tris-HCl (pH 8.0), 100 mM sodium malonate, and 30% PEG 1000 in the presence of 1 mM DTT or H_2O_2 (see Fig. 3). The C245S mutant crystals were grown under the same conditions without redox reagents (see Fig. 3). Crystals appeared within ~1 day and reached full size within 3–4 days. For data collection, the crystals were transferred to 20% PEG 200 cryoprotectant and flash-cooled in liquid nitrogen. Data were collected at beamline BL44XU of SPring-8 (Hyogo, Japan) using an MX225-HE CCD detector (Rayonix). All VSOP coiled-coil crystals belong to the $P2_12_12_1$ space group and diffracted x-rays to 1.37–1.55 Å (see Table 1). All data were processed using HKL2000 (HKL Research Inc.). The structures were solved by molecular replacement using Phaser (18) and a previously solved WT_neutral coiled-coil template (Protein Data Bank code 3VMX). Model building was done in Coot (19). The $P2_12_12_1$ space group asymmetric unit contains two dimers. We were able to build 48 residues for each of three VSOP coiled-coil chains and 47 residues for the fourth chain (of 51 residues each) for the WT crystal structures (WT_DTT and WT_H_2O_2). Two chains of 49 residues, one chain of 48 residues, and one chain of 47 residues were built in the model of C245S. All resulting models were refined using REFMAC5 (20) with the inclusion of TLS parameters throughout refinement. The coiled-coil parameters were calculated with TWISTER (21), and the coiled-coil radii are reported (see Fig. 3D).

Circular Dichroism Spectroscopy—A protein solution composed of 50 μM purified coiled-coil protein in buffer containing 150 mM KCl, 1 mM DTT/H_2O_2, and 10 mM K_2HPO_4 (pH 7.3) was analyzed using a JASCO J-715 spectropolarimeter equipped with a Peltier device. Thermal stability was assessed by monitoring the CD spectrum at 222 nm every 0.2 °C from 4 to 70 °C using a 1 °C/min temperature gradient.

Electrophysiology—The cDNA for the C245S mutant mVSOP/Hv1 channel was transfected into HEK293T cells. Macroscopic currents were recorded in the whole cell clamp configuration using an Axopatch 200B amplifier (Molecular Devices), in which 500-ms step pulses from −20 to 120 mV were applied in 20-mV increments. The external solution contained 75 mM *N*-methyl-D-glucamine, 1 mM $CaCl_2$, 1 mM $MgCl_2$, 10 mM glucose, and 180 mM HEPES (pH 7.0). The pipette solution contained 65 mM *N*-methyl-D-glucamine, 3 mM $MgCl_2$, 1 mM EGTA, and 183 mM HEPES (pH 7.0). Because activation of the Hv channel is dependent on the recording temperature (13), the temperature was controlled at 27.5 ± 2.0 °C. When the currents were recorded under the oxidized conditions, the external solution was changed to a solution containing 10 mM H_2O_2 (see Fig. 5C). External and internal solutions containing 1 mM DTT were used for recording under reduced conditions (see Fig. 5C). Data were analyzed using Clampfit (Molecular Devices) and Igor Pro (WaveMetrics Inc.) software. The activation time constant was obtained by fitting the activation phase of the outward currents with a single exponential function upon depolarization at 100 mV from the onset of the step pulse to the pulse end (see Fig. 5C).

Size Exclusion Chromatography—One-hundred microliters of isolated MBP-tagged mVSOP/Hv1 coiled coil at a concentration of 500 μM in buffer containing 250 mM KCl and 10 mM Tris (pH 7.3) were passed through a Superdex 200 HR 10/30 column (GE Healthcare) equilibrated with the same buffer on an ÄKTA purifier system at 4 °C (see Fig. 6A) (22, 23). Eluates were monitored at 280 nm over a flow rate of 0.5 ml/min. The molecular masses of the eluates were calculated using standard protein molecular mass markers (GE Healthcare).

Western Blotting—Macrophages were collected from the abdominal cavities of adult mice and dissolved in standard Laemmli buffer in the absence of reducing agents such as DTT and β-mercaptoethanol. After incubation for 5 min at 100 °C, the protein samples were separated by 12.5% SDS-PAGE, transferred to PVDF membranes, and detected using anti-mVSOP/Hv1 antibody and horseradish peroxidase-conjugated IgG secondary antibody (Fig. 1B) (24). The same protein samples incubated with 1 mM DTT or 1 mM copper phenanthroline (330 μM $CuSO_4$ + 1 mM *o*-phenanthroline) for 30 min were also analyzed (Fig. 1B). The amounts of the proteins were measured using CS Analyzer 3 (ATTO Corp.). To analyze the chemical accessibility to Cys-245 (see Fig. 6B), HEK293T cells expressing the channels were harvested and lysed in detergent-containing buffer (150 mM NaCl, 20 mM Tris-HCl (pH 7.5), and 1% *n*-dodecyl-β-D-maltopyranoside). The soluble fractions were reduced/oxidized with 1 mM DTT or 1 mM copper phenanthroline for 30 min, and 1 mM maleimide-conjugated PEG (MalPEG) 5000 was then added and incubated for 10 min. Protein samples were separated by SDS-PAGE after boiling for 5 min, and the bands were detected by Western blotting with anti-mVSOP/Hv1 antibody (see Fig. 6B).

RESULTS

We first analyzed the extent to which mVSOP/Hv1 is involved in disulfide formation in native tissue. Macrophages
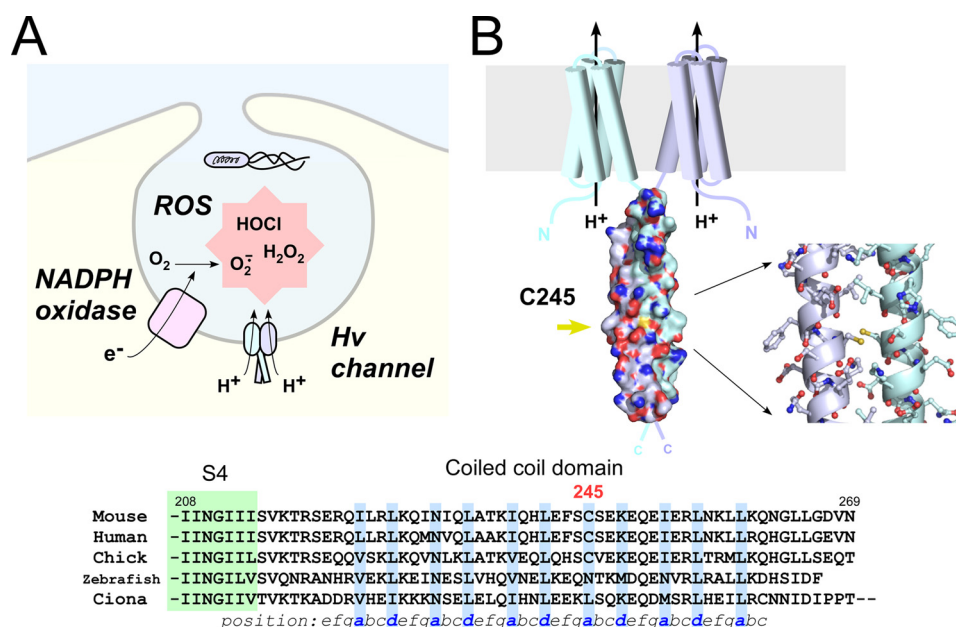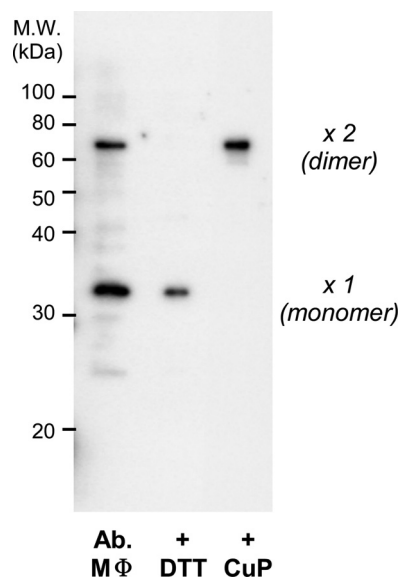
FIGURE 1. **Intersubunit disulfide bonding of Cys-245 in native mVSOP/Hv1.** *A*, schematic drawing of the Hv channel function in the phagosome. The NADPH oxidase produces ROS, and the Hv channel regulates NADPH oxidase activity. H^+ efflux through the Hv channel effectively contributes to the charge compensation for electron transfer via NADPH oxidase, which helps to sustain the production of ROS (7). *B*, structural model of the dimeric unit of mVSOP/Hv1. Shown are the protein surface of the coiled-coil domain and a stick model of Cys-245 and surrounding residues (Protein Data Bank code 3VMX) (13). Sulfur atoms of Cys-245 are colored *yellow*, and the dual conformation in the model was omitted to facilitate visualization. Also shown is the sequence alignment of the C-terminal cytoplasmic coiled-coil domain of the Hv channel from various species. Coiled-coil residues occupying hydrophobic positions *a* and *d* are shown in *blue*. The *green box* depicts part of the last transmembrane region (S4).

were collected from the abdominal cavities of adult mice, and VSOP/Hv1 proteins were separated by electrophoresis. If the proteins formed a disulfide bond, they were not dissociated by heat denaturation prior to electrophoresis, and a band of twice the molecular mass was observed (Fig. 2). Two bands were detected with anti-mVSOP/Hv1 antibody by Western blotting, and they responded fully to the redox condition (Fig. 2). These results suggest that native VSOP/Hv1 is involved in disulfide formation in some degree with high deviation (20.7 $\pm$ 8.9% ($n = 4$); dimer) (Fig. 2). Although indirect effects of other oxidative reactions in native tissues might be involved, the pair of Cys-245 residues in the assembly domain is a possible candidate for disulfide bond formation in the Hv channel dimer.

We next focused on the structural basis of disulfide bond formation between two subunits. Cys-245 is located at position *a* of the heptad repeat, suggesting that the two sulfur atoms of Cys-245 are close to each other in the coiled-coil core. Our first structure of the coiled-coil domain shows dual conformations at Cys-245 and surrounding residues (Ser-244 and Ser-246): one involves a face-to-face formation of the Cys-245 thiols without cross-linking, and the second involves a back-to-back formation (13). This suggests that the coiled-coil structure around Cys-245 is flexible and potentially forms a disulfide bond. We made two types of coiled-coil domain crystals, reduced and oxidized, at 10 °C and collected the diffraction data. The C245S mutant was also constructed, and the crystals were grown under the same conditions. Because x-ray analysis has a tendency to reduce disulfide bonds, we minimized the shooting time to 0.2 s/image to avoid the radiation reduction. Even under these conditions, the crystals diffracted x-rays at high resolution, allowing us to measure the disulfide bonds


FIGURE 2. **Detection of the intersubunit disulfide bond in native mVSOP/Hv1.** Macrophages (*M*Φ) were collected from the abdominal cavities of adult mice and dissolved in standard Laemmli buffer in the absence of reducing agents such as DTT and β-mercaptoethanol. Proteins were detected by Western blotting with anti-mVSOP/Hv1 antibody. The same protein samples incubated with DTT or copper phenanthroline (*CuP*) prior to electrophoresis were also analyzed.

(Table 1). The structures solved by molecular replacement are parallel left-handed two-stranded coiled coils with the same packing as in the previous structure (WT_neutral, Protein Data Bank code 3VMX) (Fig. 3). In the crystal structure obtained under reduced conditions (Fig. 3*A*), the distance between each sulfur atom of Cys-245 is 4.4 Å, whereas under oxidizing conditions, the distance is 2.0 Å, consistent with a disulfide bond.

TABLE 1

X-ray data correction and refinement statistics

|	WT_DTT	WT_H$_2$O$_2$	C245S
Data collection			
Resolution (Å)	50.0-1.47 (1.50-1.47)	50.0-1.55 (1.58-1.55)	50.0-1.37 (1.39-1.37)
Space group	P2$_1$2$_1$2$_1$	P2$_1$2$_1$2$_1$	P2$_1$2$_1$2$_1$
Cell dimensions			
a, b, c (Å)	40.17, 54.07, 81.54	40.31, 54.15, 81.88	40.13, 53.89, 81.41
α, β, γ	90.00°, 90.00°, 90.00°	90.00°, 90.00°, 90.00°	90.00°, 90.00°, 90.00°
R_{sym}	7.0 (49.5)	7.5 (48.0)	4.2 (48.4)
Wavelength	0.9000	0.9000	0.9000
$I/\sigma I$	41.4 (4.0)	56.8 (4.7)	59.7 (4.1)
Completeness (%)	99.6 (100)	100 (100)	100 (99.9)
Redundancy	7.2 (7.2)	12.3 (7.4)	8.3 (7.1)
Refinement			
Resolution (Å)	1.47	1.55	1.37
No. of reflections	30,921	26,774	37,776
R_{work}/R_{free}	19.8/23.4	19.3/23.3	18.1/21.8
Total No. of atoms			
Protein	1705	1659	1690
Water	239	228	242
Average B-factors (Å)	13.4	14.6	15.3
Protein			
Water	25.1	26.2	26.7
r.m.s.d.[a]			
Bond lengths (Å)	0.023	0.025	0.026
Bond angles	2.165°	2.36°	2.445°

[a] r.m.s.d., root mean square deviation.
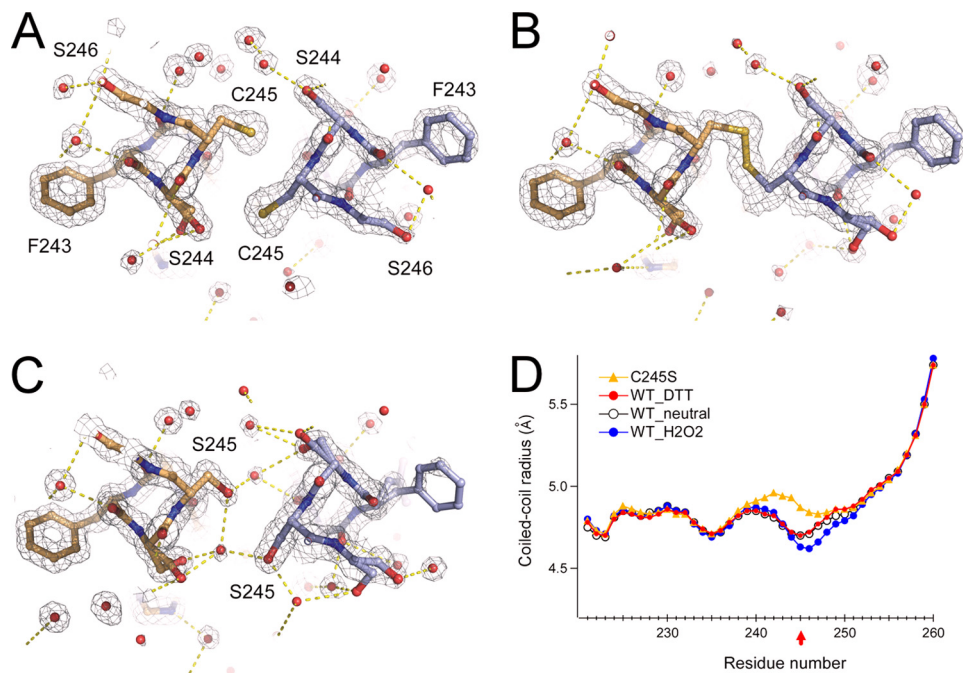
FIGURE 3. **Crystal structure analysis of the disulfide bond in the coiled coil.** *A* and *B*, structure and 2F_o − F_c maps of Cys-245 and surrounding residues in the presence of 1 mM DTT (*A*) or 1 mM H$_2$O$_2$ (*B*). *C*, structure and 2F_o − F_c maps of the C245S mutant coiled coil. *Red spheres* depict the oxygen atoms of water molecules. *Yellow dashed lines* depict polar contacts. Maps are contoured at 1.5σ. Neighboring Ser residues form a dual conformation. *D*, structural comparison of the WT_neutral (Protein Data Bank code 3VMX), WT_H$_2$O$_2$, WT_DTT, and C245S crystal structures.

The crystal structure of the C245S mutant coiled coil also shows the non-cross-linked formation and a hydroxyl group at Ser-245 making a hydrogen bond with buried water molecules (Fig. 3C). The coiled-coil radius around Cys-245 is narrowed by the disulfide bond (WT_H$_2$O$_2$) (Fig. 3D, *closed circles*), whereas that of the C245S mutant coiled coil is wider because of the water molecules in the core (Fig. 3C). The coiled-coil radii of the other regions are identical. Observation of the difference density maps at the positions of the Cys side chains ensured the adequacy of the models (Fig. 4). Thus, the cytoplasmic coiled

coil changed conformation at Cys-245 and the surrounding residues dependent on redox conditions.

The disulfide bond between two subunits possibly affects the stability of the coiled-coil assembly. The thermal stability of the coiled-coil assembly was analyzed by CD spectroscopy. The temperature dependence of the CD signal showed a cooperative loss of structure, and as indicated in a previous study (13), the melting temperature (apparent T_m = 40.6 and 40.8 °C (n = 2)) was lower than those of other naturally occurring coiled-coil proteins (T_m > 65 °C) (Fig. 5A). The T_m was shifted
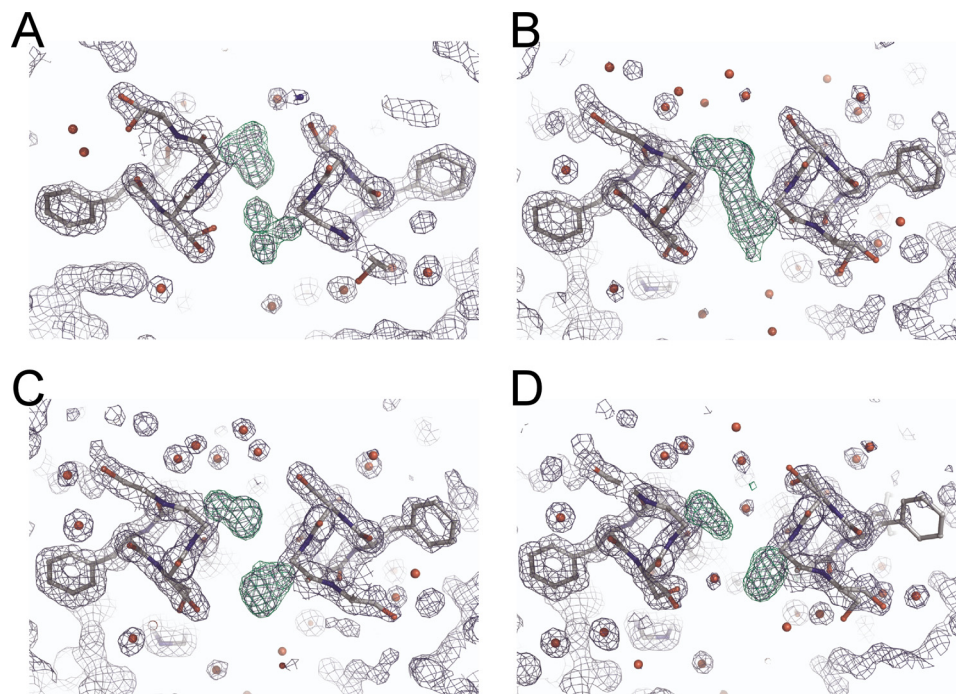
FIGURE 4. **Electron density map of the disulfide bonds.** Shown are refined structure models and electron densities of Cys-245 and surrounding residues when the Cys side chains are absent. The $2F_o - F_c$ composite omit map is contoured at 1.5σ, and the $F_o - F_c$ difference map (*green*) is contoured at 4.0σ. The clear electron densities of the dual conformation of Cys-245 (WT_neutral; *A*), the clear cross-link between Cys residues (WT_H$_2$O$_2$; *B*), and the clear separation of the densities (WT_DTT (*C*) and C245S (*D*)) are shown.

to a higher temperature (apparent T_m = 48.1 and 49.0 °C (n = 2)) by oxidation with H$_2$O$_2$ (Fig. 5*A*). The C245S mutation showed a lower T_m (apparent T_m = 30.9 and 30.4 °C (n = 2)) compared with WT_DTT and did not show the T_m shift upon oxidation (apparent T_m = 30.9 and 31.9 °C (n = 2)) (Fig. 5*B*). Thus, the intersubunit disulfide bond formed by oxidation increased the thermal stability of the coiled-coil assembly. In addition, the electrophysiological properties of the C245S mutant channel were analyzed. As expected, the activation kinetics were not changed by oxidation and reduction (Fig. 5*C*). The threshold and amplitudes were also not dependent on the redox state (data not shown). We note that the activation kinetics of the C245S mutant were similar in value to those of the WT (10, 13), suggesting that the C245S mutant channel could be a dimer on the membrane under these experimental conditions, which is consistent with the crystal structure (Fig. 3*C*). Burial of the hydrophobic residues other than those involved in the disulfide bond on the interface of the C245S coiled coil may provide the thermodynamic driving force for channel dimerization.

Because the sulfur atoms of Cys-245 are exposed on the protein surface of the coiled-coil domain (Fig. 1*B*), some accessory molecules are assumed to be able to bind to Cys-245. We next analyzed the accessibility of the thiol modifier maleimide to Cys-245. Maleimide is a chemical compound that binds to thiol and is a useful tool in biochemistry for evaluating exposed/buried Cys residues. The molecular masses of the coiled-coil proteins were analyzed by size exclusion chromatography. The molecular mass of the coiled-coil domain protein showed a single peak corresponding to a dimer (Fig. 6*A*), which is consistent with our previous results from analytical ultracentrifugation

(13). The signal peak was shifted in two steps toward the higher mass by adding MalPEG 10,000, where the lower mass peak corresponding to the monomer was not generated (Fig. 6*A*). These results suggest that two molecules of MalPEG 10,000 are able to bind to Cys-245 without the dimeric assembly collapsing. The redox dependence of the maleimide accessibility was also analyzed with the full-length channel by Western blotting. The WT mVSOP/Hv1 channel showed a monomer band after denaturation (Fig. 6*B*, *left*). Upon the addition of MalPEG 5000, the band was shifted toward the higher molecular mass (1-mer + MalPEG band), whereas only dimer bands (no 2-mer + MalPEG band) were observed upon the addition of MalPEG with copper phenanthroline pre-oxidation (Fig. 6*B*). These results suggest that maleimide cannot access Cys-245 forming a disulfide bond because of the lack of free thiols. We also tested the C245S mutant, in which neither disulfide-bonded nor MalPEG-bonded bands were detected (Fig. 6*B*, *right*). This indicates that the disulfide bond observed in the WT was derived from Cys-245, although there is another Cys at position 103 in the transmembrane region in mVSOP/Hv1. We observed two bands, a larger (major) band and a smaller (minor) band, in the monomer possibly because of translation from an alternative initiation site, and this caused triplet bands in the dimeric molecule (Fig. 6*B*). Thus, the accessibility of maleimide to Cys-245 is dependent on the redox state of the Cys-245 thiol.

DISCUSSION

In this study, we observed the formation of disulfide bonds by Cys-245 in the coiled-coil core of native mVSOP/Hv1 in abdominal macrophages (Fig. 2) and analyzed the protein biochemical properties of the disulfide bond formation. Protein
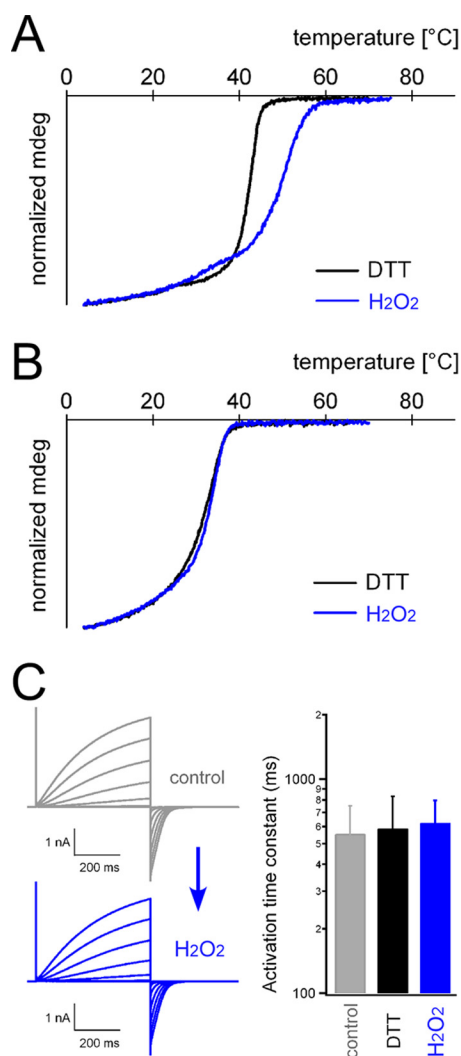
FIGURE 5. **Thermal stability of the coiled-coil domain under redox conditions.** The melting temperatures of the WT (*A*) and C245S mutant (*B*) coiled-coil proteins were analyzed by CD spectroscopy. Data for WT_DTT are from our previous study (13). *mdeg*, millidegrees. *C*, activation kinetics of the C245S mutant channel. Shown are representative current traces recorded from an identical patch before (control; *gray traces*) and after (H₂O₂; *blue traces*) oxidation. Accumulated data are shown on the *right*, and no significant statistical difference was observed. *Error bars* depict means ± S.D. (*n* = 9, 13, and 11 for the control, DTT, and H₂O₂, respectively).

crystallization and CD spectroscopy revealed that the coiled-coil domain assembly was stabilized by the disulfide bond (Figs. 3 and 5). Chemical accessibility to the exposed Cys-245 was also dependent on the redox condition (Fig. 6).

The coiled coil is the most common subunit of oligomerization motifs in proteins, in which the burial of hydrophobic residues in the core provides the thermodynamic driving force for oligomerization. Although a large number of coiled-coil motifs have been identified in natural proteins based on the amino acid sequence of the heptad repeat, only a few coiled coils contain Cys in the core alignment (16). There have been only minimal successes in the structural determination of the disulfide bond in the coiled coil. Crystal structures of *de novo* designed parallel trimeric coiled coils were determined, showing that the Cys in the core of the coiled coil forms a binding pocket suitable for heavy metals (25). In another case, the crystal structure of a bacterial DNA-binding protein shows a disulfide bond on the

dimerization interface in the core of a short antiparallel dimeric coiled coil (26). The contribution of disulfide bonds to protein stability using the dimeric GCN4 coiled coil was analyzed (17). This study showed that the disulfide bond at core position a destabilizes the coiled coil, whereas that at position d stabilizes the coiled coil (17). Computational modeling demonstrated that the disulfide bond at position a causes a stereochemical change in the polypeptide backbone along the entire coiled-coil structure (17). In contrast, in our present study, the crystal structures show that the disulfide bond at Cys-245 (at position a) stabilizes the coiled coil with a small local structural change around Cys-245, which is similar to the stabilizing effect of the disulfide bond at position d in the previous GCN4 study. As discussed in the previous study (17), coiled-coil protein stability is significantly dependent on the geometric strain mediated by the disulfide bond and the local/general flexibility of the molecule. The hydrophobic effect against the polar solvent is generally a key determinant of protein stability. In fact, our crystallographic analysis showed that there is some local flexibility at Cys-245 and surrounding residues, including hydrophilic residues (Lys-248) at core position d. Increased packing of two strands by the disulfide bond without the entire disruption of the coiled coil owing to the local flexibility (Fig. 3*D*) may increase the stability of the coiled coil. Flexibility around Cys-245 also allows binding of two molecules of maleimide without disruption of the dimeric assembly. The side-open structure consisting of the small hydrophilic residues Ser-244 and Ser-246 around Cys-245 may also contribute to the accessibility.

The structural characteristics of the redox sensitivity of the mVSOP/Hv1 coiled coil may have some physiological significance. We observed in this study that a certain percentage of mVSOP/Hv1 harvested from the native macrophages underwent disulfide formation. In contrast, following heterologous expression in HEK293 cells, the disulfide bond was not observed unless the cells were exposed to oxidizing conditions (Fig. 6*B*, *left*), demonstrating the native oxidation capacity of macrophages (Fig. 2). The Hv channel is expressed in phagocytes (27), where ROS production for phagocytic events causes fluctuations in oxidation-reduction. Stabilization of the coiled-coil domain by disulfide formation and subsequent stabilization of the channel dimerization might serve as the feedback system for ROS production. ROS elicit cellular toxicity that causes disease (2–4), and therefore, several feedback systems directly or indirectly involving VSOP/Hv1 might exist in the phagosome. In addition, phagocytes migrate into inflamed tissues, where the temperature is higher than in other regions. We have shown that the thermal stability of the coiled-coil domain of mVSOP/Hv1 is essentially weak and that the coiled coil unfolds at a temperature slightly higher than body temperature (~40 °C when reduced) (Fig. 5). Furthermore, the temperature dependence of coiled-coil unfolding is altered by the redox state. Hv channels might dissociate and associate on the phagosomal membrane dependent on the surrounding environment. The physiological significance of the dimerization of Hv channels has not been fully determined. Previous studies reported that monomeric channels (clones ΔNΔC and ΔC) that were constructed by deletion of the whole cytoplasmic domain or the
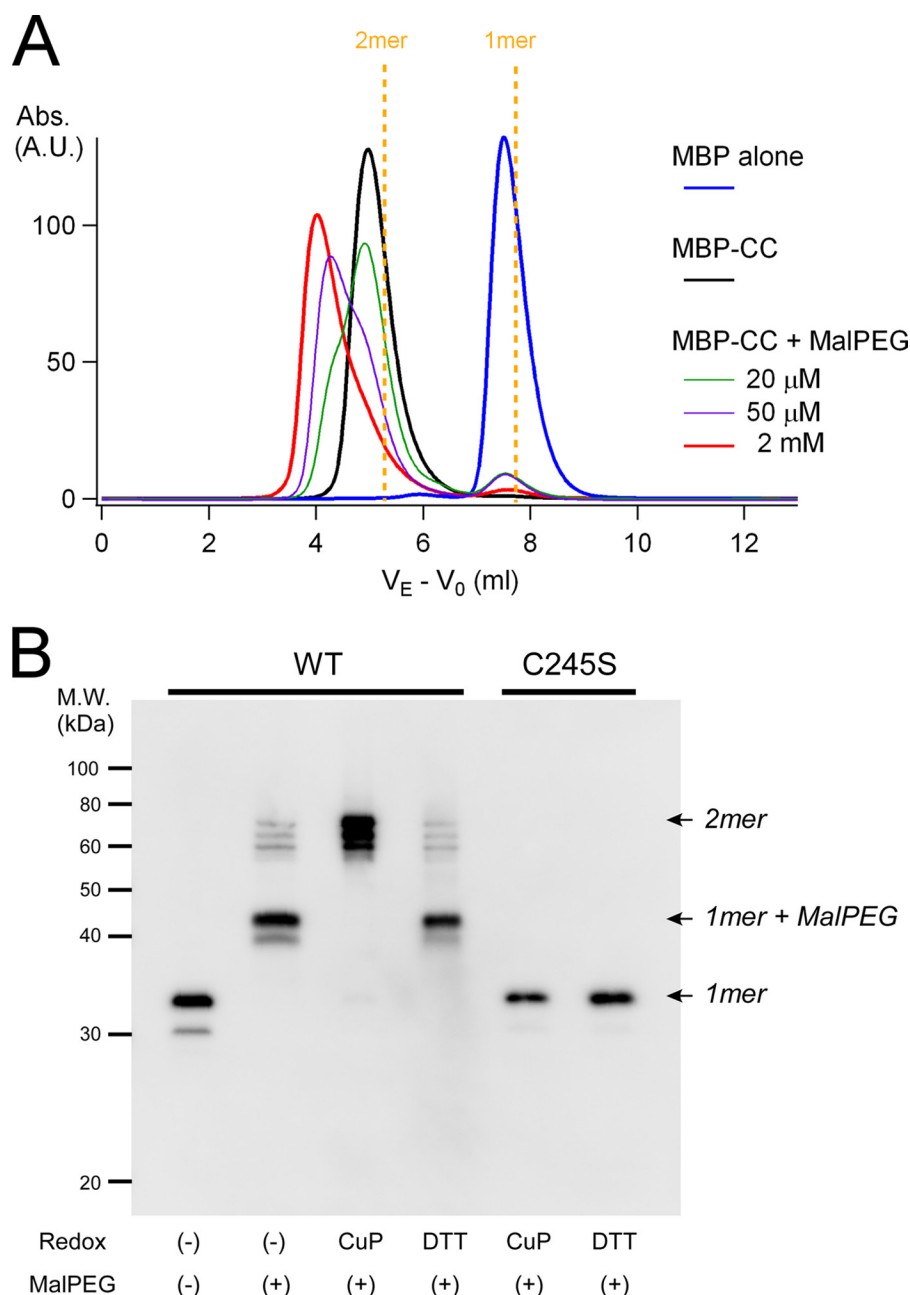
FIGURE 6. **Analysis of accessibility to Cys-245 under redox conditions.** *A*, the chemical accessibility of maleimide to Cys-245 in the coiled-coil proteins was analyzed by size exclusion chromatography. Protein samples were mixed with various concentrations of MalPEG 10,000 (20 μM (*green*), 50 μM (*purple*), and 2 mM (*red*)) and incubated for 1 h at 4 °C prior to analysis. Signals were derived from the eluates for MBP (45 kDa), the MBP-tagged coiled-coil protein (*MBP-CC*; 51 kDa), and the MBP-tagged coiled-coil protein bound to MalPEG 10,000 (51 + $n \times$ 10 kDa (n = 1 or 2)). MalPEG itself did not show any signal, and MBP does not contain Cys. V_E is corrected for void elution volume by subtracting that of blue dextran (V_0). *Dashed yellow lines* indicate the predicted elution profiles of the MBP-tagged dimeric and monomeric coiled-coil proteins. *A.U.*, absorbance units. *B*, maleimide accessibility to Cys-245 in the coiled-coil domain of full-length mVSOP/Hv1 WT and C245S mutant channels under redox conditions was analyzed by Western blotting. Redox conditions are indicated. *CuP*, copper phenanthroline.

coiled-coil domain show different gating properties compared with the dimeric WT channel (10, 13). The monomeric channels show accelerated activation kinetics with a lack of the gating cooperativity within the dimer (13–15). Therefore, if switching between dimer and monomer occurs on the membrane, the redox-dependent stabilization of the coiled-coil domain may play important roles in cell function. The long-term redox imbalance might influence the channel multimerization, and real-time monitoring of the Hv channels in rela-

tion to redox state will be addressed in the future. It has also been reported that the coiled-coil domain of VSOP/Hv1 determines the localization of channels in cells (28). Thus, the redox sensitivity of the coiled-coil domain may affect these functions and lead to altered cell function. Furthermore, unidentified active substances may bind to Cys-245 in a redox-dependent manner to play certain physiological roles. Cell physiological analysis focusing on the redox dependence of the coiled-coil structure will be informative.

REFERENCES

1. Devasagayam, T. P., Tilak, J. C., Boloor, K. K., Sane, K. S., Ghaskadbi, S. S., and Lele, R. D. (2004) Free radicals and antioxidants in human health: current status and future prospects. *J. Assoc. Physicians India* **52,** 794–804

2. Waris, G., and Ahsan, H. (2006) Reactive oxygen species: role in the development of cancer and various chronic conditions. *J. Carcinog.* **5,** 14

3. Su, B., Wang, X., Nunomura, A., Moreira, P. I., Lee, H. G., Perry, G., Smith, M. A., and Zhu, X. (2008) Oxidative stress signaling in Alzheimer's disease. *Curr. Alzheimer Res.* **5,** 525–532

4. Sahinoglu, T., Stevens, C. R., Bhatt, B., and Blake, D. R. (1996) The role of reactive oxygen species in inflammatory disease: evaluation of methodology. *Methods* **9,** 628–634

5. Rada, B., and Leto, T. L. (2008) Oxidative innate immune defenses by Nox/Duox family NADPH oxidases. *Contrib. Microbiol.* **15,** 164–187

6. El Chemaly, A., and Demaurex, N. (2012) Do Hv1 proton channels regulate the ionic and redox homeostasis of phagosomes? *Mol. Cell. Endocrinol.* **353,** 82–87

7. Decoursey, T. E. (2003) Voltage-gated proton channels and other proton transfer pathways. *Physiol. Rev.* **83,** 475–579

8. Ramsey, I. S., Moran, M. M., Chong, J. A., and Clapham, D. E. (2006) A voltage-gated proton-selective channel lacking the pore domain. *Nature* **440,** 1213–1216

9. Sasaki, M., Takagi, M., and Okamura, Y. (2006) A voltage sensor-domain protein is a voltage-gated proton channel. *Science* **312,** 589–592

10. Koch, H. P., Kurokawa, T., Okochi, Y., Sasaki, M., Okamura, Y., and Larsson, H. P. (2008) Multimeric nature of voltage-gated proton channels. *Proc. Natl. Acad. Sci. U.S.A.* **105,** 9111–9116

11. Lee, S. Y., Letts, J. A., and Mackinnon, R. (2008) Dimeric subunit stoichiometry of the human voltage-dependent proton channel Hv1. *Proc. Natl. Acad. Sci. U.S.A.* **105,** 7692–7695

12. Tombola, F., Ulbrich, M. H., and Isacoff, E. Y. (2008) The voltage-gated proton channel Hv1 has two pores, each controlled by one voltage sensor. *Neuron* **58,** 546–556

13. Fujiwara, Y., Kurokawa, T., Takeshita, K., Kobayashi, M., Okochi, Y., Nakagawa, A., and Okamura, Y. (2012) The cytoplasmic coiled-coil mediates cooperative gating temperature sensitivity in the voltage-gated H$^+$ channel Hv1. *Nat. Commun.* **3,** 816

14. Gonzalez, C., Koch, H. P., Drum, B. M., and Larsson, H. P. (2010) Strong cooperativity between subunits in voltage-gated proton channels. *Nat. Struct. Mol. Biol.* **17,** 51–56

15. Tombola, F., Ulbrich, M. H., Kohout, S. C., and Isacoff, E. Y. (2010) The opening of the two pores of the Hv1 voltage-gated proton channel is tuned by cooperativity. *Nat. Struct. Mol. Biol.* **17,** 44–50

16. Vinson, C., Myakishev, M., Acharya, A., Mir, A. A., Moll, J. R., and Bonovich, M. (2002) Classification of human b-ZIP proteins based on dimerization properties. *Mol. Cell. Biol.* **22,** 6321–6335

17. Zhou, N. E., Kay, C. M., and Hodges, R. S. (1993) Disulfide bond contribution to protein stability: positional effects of substitution in the hydrophobic core of the two-stranded α-helical coiled-coil. *Biochemistry* **32,** 3178–3187

18. Storoni, L. C., McCoy, A. J., and Read, R. J. (2004) Likelihood-enhanced fast rotation functions. *Acta Crystallogr. D Biol. Crystallogr.* **60,** 432–438

19. Emsley, P., and Cowtan, K. (2004) Coot: model-building tools for molecular graphics. *Acta Crystallogr. D Biol. Crystallogr.* **60,** 2126–2132

20. Murshudov, G. N., Vagin, A. A., and Dodson, E. J. (1997) Refinement of macromolecular structures by the maximum-likelihood method. *Acta Crystallogr. D Biol. Crystallogr.* **53,** 240–255

21. Strelkov, S. V., and Burkhard, P. (2002) Analysis of α-helical coiled coils with the program TWISTER reveals a structural mechanism for stutter compensation. *J. Struct. Biol.* **137,** 54–64

22. Howard, R. J., Clark, K. A., Holton, J. M., and Minor, D. L., Jr. (2007) Structural insight into KCNQ (Kv7) channel assembly and channelopathy. *Neuron* **53,** 663–675

23. Fujiwara, Y., Kurokawa, T., Takeshita, K., Nakagawa, A., Larsson, H. P., and Okamura, Y. (2013) Gating of the designed trimeric/tetrameric voltage-gated H$^+$ channel. *J. Physiol.* **591,** 627–640

24. Sakata, S., Kurokawa, T., Nørholm, M. H., Takagi, M., Okochi, Y., von Heijne, G., and Okamura, Y. (2010) Functionality of the voltage-gated proton channel truncated in S4. *Proc. Natl. Acad. Sci. U.S.A.* **107,** 2313–2318

25. Chakraborty, S., Touw, D. S., Peacock, A. F., Stuckey, J., and Pecoraro, V. L. (2010) Structural comparisons of apo- and metalated three-stranded coiled coils clarify metal binding determinants in thiolate containing designed peptides. *J. Am. Chem. Soc.* **132,** 13240–13250

26. Shinkai, A., Sekine, S., Urushibata, A., Terada, T., Shirouzu, M., and Yokoyama, S. (2007) The putative DNA-binding protein Sto12a from the thermoacidophilic archaeon *Sulfolobus tokodaii* contains intrachain and interchain disulfide bonds. *J. Mol. Biol.* **372,** 1293–1304

27. Okochi, Y., Sasaki, M., Iwasaki, H., and Okamura, Y. (2009) Voltage-gated proton channel is expressed on phagosomes. *Biochem. Biophys. Res. Commun.* **382,** 274–279

28. Li, S. J., Zhao, Q., Zhou, Q., Unno, H., Zhai, Y., and Sun, F. (2010) The role and structure of the carboxyl-terminal domain of the human voltage-gated proton channel Hv1. *J. Biol. Chem.* **285,** 12047–12054